

1 research article for Marine Ecology Progress Series

2 3 **Benthic O₂ uptake by coral gardens at the Condor seamount (Azores)**

4
5 Lorenzo Rovelli^{1,8*}, Marina Carreiro-Silva^{2,3}, Karl M. Attard^{1,4,5}, Maria Rakka^{2,3}, Carlos Dominguez-
6 Carrió^{2,3}, Meri Bilan^{2,3}, Sabena Blackbird⁶, Telmo Morato^{2,3}, George A. Wolff⁶, Ronnie N. Glud^{1,5,7}

7
8 ¹HADAL & Nordcee, Department of Biology, University of Southern Denmark, 5230 Odense M, Denmark

9 ²IMAR – Instituto do Mar, Universidade dos Açores, 9901-862 Horta, Portugal

10 ³Instituto de Investigação em Ciências do Mar – Okeanos, Universidade dos Açores, 9901-862 Horta,
11 Portugal

12 ⁴Tvärminne Zoological Station, University of Helsinki, 10900 Hanko, Finland

13 ⁵Danish Institute of Advanced Study – DIAS, University of Southern Denmark, 5230 Odense M, Denmark

14 ⁶School of Environmental Sciences, University of Liverpool, L69 3GP Liverpool, United Kingdom

15 ⁷Department of Ocean and Environmental Sciences, Tokyo University of Marine Science and Technology,
16 108-8477 Tokyo, Japan

17 ⁸now at iES – Institute for Environmental Sciences, University of Koblenz-Landau, 76829 Landau, Germany

18 *corresponding author

19 20 21 **Short title**

22 Oxygen uptake by coral gardens

23 24 **Abstract**

25 Using the non-invasive aquatic eddy covariance (AEC) technique, we provide the first oxygen (O₂)
26 uptake rates from within coral gardens at the Condor seamount (Azores). To explore some of the key drivers
27 of the benthic O₂ demand, we obtained benthic images, quantified local hydrodynamics, estimated
28 phototrophic biomass and deposition dynamics with a long-term moored sediment trap. The coral gardens
29 were dominated by the octocorals *Viminella flagellum* and *Dentomuricea* aff. *meteor*. Daily rates of O₂
30 uptake within three targeted coral garden sites (203 – 206 m depth) ranged from 10.0 ± 0.88 to 18.8 ± 2.0
31 mmol m⁻² d⁻¹ (mean ± standard error) and were up to ten times higher than two local sandy reference sites
32 within the seamount summit area. The overall mean O₂ uptake rate for the garden (13.4 mmol m⁻² d⁻¹) was
33 twice the global mean for sedimentary habitats at comparable depths. Combined with parallel *ex situ*
34 incubations, the results suggest that the octocorals might contribute just ~5% of the observed O₂ uptake rates.
35 Deposition of particulate organic matter (POM) assessed by the sediment trap accounted for less than 10% of
36 the O₂ demand of the coral garden, implying a substantial POM supply circumventing the deployed traps.
37 Our results expand the database for carbon turnover rates in cold-water coral (CWC) habitats by including
38 the first estimates from these largely under-studied coral gardens.

39 40 **Keywords**

41 Aquatic eddy covariance, cold-water corals, Condor seamount, community oxygen uptake, *Viminella*
42 *flagellum*, *Dentomuricea* aff. *meteor*.

43 **1. Introduction**

44 Cold-water corals (CWCs) are important ecosystem engineers at continental shelves, slopes, seamounts
45 and ridge systems (Roberts et al. 2006, 2009). Habitats formed by CWCs include reefs produced by
46 Scleractinia species (stony corals), and coral gardens formed by Alcyonacea (gorgonians and soft corals),
47 Antipatharia (black corals) and Stylasteridae (lace corals) (Buhl-Mortensen & Buhl-Mortensen 2018). These
48 communities enhance biodiversity and biomass at the deep seafloor by providing complex three-dimensional
49 structures used as shelter, breeding and feeding grounds for other organisms (Buhl-Mortensen et al. 2010,
50 2017, Henry & Roberts 2017). The extent and complexity of CWC reefs formed by stony corals have been
51 intensively studied (Davies & Guinotte 2011) and their role as hotspots of carbon and nitrogen cycling in the
52 North Atlantic has been documented by a number of studies (van Oevelen et al. 2009, White et al. 2012,
53 Rovelli et al. 2015, Cathalot et al. 2015, de Froe et al. 2019, De Clippele et al. 2021). In contrast, and despite
54 their widespread occurrence, the importance of coral gardens remains largely unexplored (Yesson et al.
55 2012, Rossi et al. 2017, Buhl-Mortensen & Buhl-Mortensen 2018).

56 Traditionally, the importance of CWC habitats for benthic carbon cycling has been assessed by *ex situ*
57 and *in situ* incubations of coral fragments (Dodds et al. 2007, Khripounoff et al. 2014) or sub-samples taken
58 from the CWC community (de Froe et al. 2019). However, this invasive approach can change important
59 hydrodynamic drivers and thus only poorly represents the complex three-dimensional structures that make
60 up these natural communities. To overcome such shortcomings, non-invasive approaches, most notably open
61 water based dissolved oxygen (O₂) budget methods (see White et al. 2012) and the aquatic eddy covariance
62 (AEC) technique (Rovelli et al. 2015, Cathalot et al. 2015, de Froe et al. 2019) have been applied. Open-
63 water approaches are limited to settings with a constrained hydrodynamic regime, e.g., canyon-like settings
64 with a dominant flow direction and quantifiable water residence time and are thus not ideal for natural CWC
65 habitats, which are often characterized by complex hydrodynamics. In contrast, the AEC technique is more
66 widely applicable to CWC reefs, tropical reefs and other complex benthic ecosystems where it has provided
67 spatially and temporally integrated assessments of the O₂ exchange (Long et al. 2013, Rovelli et al. 2015,
68 2019, Cathalot et al. 2015), and ultimately contributed to advance our understanding of the local carbon
69 turnover for those habitats.

70 In this study, we applied AEC to quantify and characterize the O₂ uptake rates of a coral garden formed
71 by the octocorals *Viminella flagellum* and *Dentomuricea* aff. *meteor* on the summit of Condor seamount
72 (Azores). The island slope and seamount habitats of the Azores are mostly dominated by coral gardens
73 (Tempera et al. 2012, 2013), which are key communities for regional biodiversity and potentially for carbon
74 and nutrient cycling (Porteiro et al. 2013, Carreiro-Silva et al. 2017, Gomes-Pereira et al. 2017).
75 Measurements of community respiration rates were complemented with (i) octocoral density data obtained
76 from underwater images, (ii) water column profiling (e.g., temperature, turbidity, chlorophyll a), (iii) discrete
77 water samples to characterize nutrient availability and suspended particulate organic matter (POM) and (iv)

78 data from a sediment trap mooring to investigate POM supply to the seamount. This study aims to provide
79 insights on the importance of octocoral gardens for benthic carbon cycling in this important oceanic region.
80

81 2. Material and Methods

82 2.1. Study site

83 Condor seamount is a linear volcanic ridge situated 17 km south-west of Faial island, in the Azores
84 archipelago, in the north-east Atlantic (Fig. 1). The seamount measures 39 km in length and rises from 2000
85 m to a flattened summit at 184 m water depth (Tempera et al. 2013). The summit area (<300 m depth)
86 encompasses an approximate surface of 6.85 km² (Pham et al. 2013). Benthic habitats consist of
87 unconsolidated sandy sediments transitioning to hard substrates, covering up to 80% of the summit area.
88 Hard-substrate habitats are characterized by the presence of coral gardens, mostly dominated by the
89 octocorals *Viminella flagellum* and *Dentomuricea* aff. *meteor* (Tempera et al. 2012, Porteiro et al. 2013).
90 Although monospecific coral gardens of *V. flagellum* and *D.* aff. *meteor* are also present within the summit
91 area, the most prominent gardens encompass both coral species, often in conjunction with tall hydrozoans,
92 e.g., *Polyplumaria flabellata* and *Lytocarpia myriophyllum* (Tempera et al. 2012). The seamount induces a
93 anticyclonic Taylor cap over the summit, i.e., an enclosed circulation with mean near-bottom flow velocities
94 of ~4 cm s⁻¹ (Bashmachnikov et al. 2013), which might promote the retention of organic matter and enhance
95 local productivity (see White et al. 2008). The water column above the seamount is characterized by strong
96 seasonal dynamics in salinity, dissolved oxygen (O₂) and chlorophyll *a* (Chl. *a*) concentrations which is also
97 reflected in the zooplankton and phytoplankton abundance and distribution (Carmo et al. 2013, Santos et al.
98 2013).

99 100 2.2 Selection of sites for AEC deployments, coral densities and sizes

101 Video images used to select suitable areas for aquatic eddy covariance (AEC) deployments were recorded
102 by means of the towed camera system from the R/V Pelagia (NIOZ) during the 2016 MIDAS cruise (Cruise
103 code 64PE413). The underwater video device was equipped with a high-definition camera (1920x1080
104 pixels) facing downwards, a pair of parallel lasers 30 cm apart used for image scaling and an ultra-short
105 baseline (USBL) positioning system to acquire accurate geopositioning data from the vehicle when cruising
106 underwater. Only sequences recorded in the summit area of the seamount (<260 m depth) were considered
107 for this study (Dive H04, white stripped lines in Fig. 1a). Two main locations were identified: areas
108 characterized by the presence of dense coral gardens (Fig. 1c-d) and areas with bare sand with no
109 distinguishable epifauna, such as corals and hydrozoans (Fig. 1e). AEC deployments were performed in July
110 and early August of 2018 during short daytrips with the vessel L/V Águas Vivas (University of the Azores).
111 Three AEC deployments were performed over the selected coral garden (AEC 2,3,5), one deployment on a
112 sandy patch close to the coral garden (AEC 4, ~100 m off-site) and one more deployment (AEC 1) on a large
113 sandy area located 1.4 km away from the coral location (Fig. 1b).

114 The coral garden selected was located at a depth of ~210 m on the western part of the summit (38°
115 32.381' N, 29° 02.349' W; Fig. 1). The patch stretched for ~95 meters and was dominated by the octocoral

116 species *V. flagellum* and *D. aff. meteor*. Densities of both species were estimated using the projection of the
117 parallel lasers over the seafloor, which allowed for a fixed field of view of 2 m to be delimited along the path
118 of the camera system over the coral patch (total area evaluated: 190 m²). All octocoral colonies observed
119 within the field of view were annotated, and species counts were converted into density estimates by
120 dividing the length of the patch into a string of 10 m² sampling units. The average sizes for both coral species
121 were estimated using underwater video images recorded with the mini-ROV SP (SeaBotix LBV300S-6;
122 IMAR-DOP/UAz), equipped with a standard-definition camera (570 lines) and parallel lasers 5 cm apart.
123 The 8 ROV dives used for this study were performed on coral aggregations at the summit of Condor
124 seamount (175-250 m depth) in years 2010-2011 as part of the CoralFISH project. When the reflection of the
125 parallel lasers crossed the base of the corals, video frames were extracted for coral size estimation. A total of
126 345 *V. flagellum* and 212 *D. meteor* were measured using the software Macnification (Orbicule Inc.) from a
127 total of 315 video frames extracted from the video footage.

128

129 2.3. Water column characterization

130 Water column profiles of temperature, salinity, pressure, turbidity (Seapoint Sensor Inc., USA),
131 photosynthetically active radiation (LI-193SA spherical quantum sensor; Li-COR Biosciences, USA) and
132 fluorescence (Cyclops-7; Turner Designs, USA) were collected with a CTD90M multiparameter probe (Sea
133 & Sun Technology, Germany). Measurements were conducted during a set of up to four casts before and
134 after each AEC deployment. In addition, a 5L Niskin bottle, mounted 2.5 m above the probe, was used for
135 discrete water sampling. Water samples were analyzed for dissolved nutrients, chlorophyll *a* (Chl. *a*) and
136 particulate organic matter (POM) concentrations at a depth of ~5 m above the summit (206-212 m depth) and
137 within the deep chlorophyll maximum (DCM) at approximately 50 m depth, as indicated by the values of the
138 fluorometer. Each set of CTD casts yielded a total 2 x 5 L of seawater for each targeted depth.

139 Water samples for nutrient characterization (2 x 20 mL for each set of casts) were filtered onboard using
140 0.2 µm sterile syringe filters and stored at 0 °C under dark conditions for further analyses. The concentration
141 of nitrite (NO₂⁻), nitrate (NO₃⁻), ammonium (NH₄⁺) and orthophosphate (PO₄³⁻) were determined
142 spectrophotometrically with an automatic continuous segmented flow analyzer (Skalar san^{plus}; Skalar
143 Analytical B.V., Netherlands). For POM determination, 5 L of seawater per set of casts was filtered through
144 a pre-combusted GF/F filter (0.7 µm; Whatman, United Kingdom). The filters were freeze-dried and kept at -
145 20°C pending further analyses. The concentration of particulate nitrogen (PN), particulate organic carbon
146 (POC) and particulate inorganic carbon (PIC) were quantified in duplicate using a Flash Smart CHN
147 elemental analyzer (Thermo Fisher Scientific, USA) on aliquots of known area (*ca.* 130 mm²) (see
148 Kiriakoulakis et al. 2004). Determination of Chl. *a* was performed with a spectrophotometer after filtering 3
149 L of seawater through 0.7 µm GF/F filters and subsequent extraction into acetone following Holm-Hansen et
150 al. (1965).

151

152 2.4. Benthic oxygen uptake

153 Benthic O₂ uptake was quantified by the non-invasive aquatic eddy covariance (AEC) technique. The
154 AEC system used in this study consisted of a deep-sea rated Acoustic Doppler velocimeter (Vector; Nortek
155 A/S, Norway), one O₂ microelectrode module (see McGinnis et al. 2011), one O₂ optode module
156 (Pyroscience, Germany) (see Huettel et al. 2020), and underwater battery canisters mounted on a steel frame.
157 The parallel O₂ microelectrode and optode modules were deployed concurrently to allow for redundancy and
158 cross-validation. A conductivity-temperature-depth (CTD) probe (SBE19; Seabird, United States) logger
159 equipped with an O₂ optode (Aanderaa, Denmark) was mounted on the AEC frame to collect auxiliary
160 timeseries of O₂ to calibrate the readings of the AEC microsensors. The AEC frame was also equipped with
161 two Nautilux Custom underwater LED lights and two Benthic2 camera housings (Group B Distribution Inc.,
162 United States) with GoPro Hero 3 and 4 action cameras (GoPro Inc., United States). The cameras covered
163 two of the three sides of the AEC frame and were used to visually inspect the benthic habitats and to
164 crosscheck the positioning within the targeted habitats.

165 Given the rugged nature of the seafloor, the AEC measurement height (h) was fixed to 0.35 m. High-
166 resolution (64 Hz) timeseries of current velocity and O₂ timeseries were processed for flux extraction
167 following validated data-processing protocols (see Attard et al. 2014, Rovelli et al. 2015). The timeseries
168 were averaged and despiked after Goring & Nikora (2002) to reduce the dataset sizes and instrument noise,
169 respectively. The flow velocity coordinate system was rotated using a planar fit algorithm to minimize non-
170 turbulent (advective) flow contributions over complex topographical features (Lorke et al. 2013). Turbulent
171 fluctuations of O₂ and vertical velocity were computed over a time interval of 5 min *via* linear detrending.
172 For the investigated studies, a stepwise analysis of the window size vs. mean flux (see Attard et al. 2014)
173 indicated that a 5-min window was an optimal trade-off between including the major turbulent contributions
174 while minimizing the inclusion of non-turbulent processes. Linear detrending, alignment of the O₂ and
175 velocity time series (*i.e.*, time shift), as well as the O₂ flux extraction were computed using the Fortran
176 program suite Sulfide-Oxygen-Heat Flux Eddy Analysis (SOHFEA) version 2.0 (available from
177 www.dfmcginnis.com/SOHFEA; McGinnis et al. 2014). The mean time shift was computed for each time
178 window based on the highest correlation and ranged from -0.8 to -1.2 seconds, in line with the observed low
179 flow velocities (about 2 to 7 cm s⁻¹ on average). In order to better relate the obtained O₂ flux rates to the
180 targeted benthic communities and their heterogeneity, the size of the theoretical AEC footprint area (*i.e.*, the
181 area that contributes to 90% of the flux) and the region of maximum flux contribution (X_{\max}) were estimated
182 for each deployment based on h and the bottom roughness length scale (z_0) (Berg et al. 2007). Mean values
183 for z_0 were derived from Reynolds stress assuming Law-of-the-Wall, as described in Inoue et al. (2011). It
184 should be noted that the model of Berg et al. (2007) was applied here outside of the original range of h and
185 z_0 , as in other high roughness settings (e.g., Reidenbach et al. 2013, Berg et al. 2019) and might thus be

186 subject to higher uncertainties, as the location of the footprint, and thus the associated integrated flux, shifts
187 with changes in the flow direction (Berg et al. 2007, Rodil et al. 2019, de Froe et al. 2019). While a
188 traditional flux-direction-velocity analysis, based on correlation plots and principal component analysis was
189 also performed at the coral garden sites using OriginPro® (OriginLab), our benthic mapping did not allow a
190 comprehensive assessments of flow directions, and associated AEC footprint, with footprint specific
191 biodiversity characterization (e.g., Rodil et al. (2019). Instead we characterized single habitats within each site
192 using a cumulative flux approach (see de Froe et al. 2019). Here we parsed together time periods with stable
193 flux contributions, i.e., periods in which the cumulative flux showed a clear linear trend (see Fig. S1 in the
194 Supplement). Depending on flow characteristics (direction and velocity) and benthic faunal densities, the
195 resulting mean flux might include more than one directional footprint, typically over a 30-90° range and
196 occasionally >90°, and thus provide a better spatial integration of each habitat. Periods characterized by
197 evident deviations from linear trends in the cumulative flux, e.g., spikes and step-like features which would
198 suggest unstable flux conditions, were flagged and not included in subsequent calculations. Mean O₂ uptake
199 rates were reported for the single habitats (for the garden sites) as above, based on the obtained fluxes (in 5-
200 min steps) as well as for the whole site (garden and sandy sites), by averaging all stable flux contributions
201 during the entire deployment time. To allow for better comparability with the literature, the uptake rates are
202 presented in mmol m⁻² d⁻¹. The methodological aspects of AEC applications to CWC habitats have already
203 been evaluated in detail in previous studies (Rovelli et al. 2015, de Froe et al. 2019) and such aspects will
204 only be discussed in general terms in this study.

205

206 2.5. Sediment trap

207 A mooring containing a single cone-shaped sediment trap mounted above an acoustic release was
208 deployed on the summit of Condor seamount (38° 31.2426' N, 28° 59.8488' W; Fig. 1a) on 28 November
209 2017 at a depth of 218 m. The sediment trap was located ~5 m above the bottom. The trap had a surface area
210 of 0.5 m² and contained a total of 20 bottles, filled with 2% formaldehyde in a 40 ppt salinity solution. The
211 trap was programmed to collect 20 samples from 1 December 2017 until its retrieval on 7 June 2018 (Table
212 S1). The supernatant in the retrieved bottles was decanted and replaced with a 4% formaldehyde solution and
213 stored for further treatment following Lampitt et al. (2001). Briefly, the samples were filtered, frozen and
214 freeze-dried and the dry mass recorded. POC content was measured on a Thermo Scientific FlashSmart
215 Elemental Analyser (ThermoFisher Scientific, USA), the samples being de-carbonized prior to analysis
216 (Yamamuro & Kayanne 1995). POC fluxes were calculated by dividing each bottle's carbon content by the
217 trap area and the number of days the bottle had been open.

218

219 **3. Results**

220 3.1. Coral densities and sizes in the selected coral garden

221 A total of 438 *Viminella flagellum* and 168 *Dentomuricea* aff. *meteor* colonies were annotated in the
222 targeted, 95-m-long coral garden. For *V. flagellum*, this corresponded to an average density of 2.30 ± 1.44
223 col m^{-2} (mean \pm standard deviation) and a maximum density inside the patch of 5.7 col m^{-2} . For *D. aff.*
224 *meteor*, the average density was $0.88 \pm 0.41 \text{ m}^{-2}$ with a maximum density inside the patch of 1.8 col m^{-2} . The
225 average colony sizes determined from the images recorded with the towed camera system on the seamount
226 summit were $79.8 \pm 38.2 \text{ cm}$ (mean \pm sd) for *V. flagellum* and $36.2 \pm 18.9 \text{ cm}$ for *D. aff. meteor*.

227

228 3.2. Water column

229 A total of 36 CTD casts were performed during the observational period (6 July to 1 August 2018). Mean
230 temperature ranged from $22.4 \text{ }^{\circ}\text{C}$ near the surface (4-5 m depth) to $15.0 \text{ }^{\circ}\text{C}$ near the seamount summit (~ 200
231 m depth). Salinity changed very little with depth, ranging from 36.2 to 36.0, with most variability in the 0 to
232 80 m depth range (Fig. 2). Mean photosynthetic active radiation (PAR) declined exponentially from 1200
233 $\mu\text{mol quanta m}^{-2} \text{ s}^{-1}$ at the surface to $< 2 \mu\text{mol quanta m}^{-2} \text{ s}^{-1}$ at the seamount summit. Water turbidity was
234 generally low (0.1 to 0.5 NTU), but slightly higher levels were encountered near the surface and at a depth of
235 35 m. The deep chlorophyll maximum (DCM) was located between 46 and 72 m depth and revealed a mean
236 Chl. *a* concentration of $0.9 \mu\text{g L}^{-1}$ (Fig. 2, Table 1). Surface and near-bottom Chl. *a* concentrations amounted
237 to $\leq 0.1 \mu\text{g L}^{-1}$.

238 Discrete sampling showed low concentrations of NH_4^+ (0.6 to $0.8 \mu\text{mol L}^{-1}$) in both the DCM and near
239 the bottom. As expected, nitrate (NO_3^-) concentrations, were higher near the bottom ($6.0 \mu\text{mol L}^{-1}$ on
240 average) than within the DCM ($1.1 \mu\text{mol L}^{-1}$), while NO_2^- was below detection ($< 0.1 \mu\text{mol L}^{-1}$) at both
241 depths (Table 1). Concentrations of orthophosphate (PO_4^{3-}) ranged from 0.1 to $0.4 \mu\text{mol L}^{-1}$ between the
242 DCM and near-bottom samples. The concentrations of particulate organic carbon (POC) and particulate
243 nitrogen (PN) within the DCM were on average $3.7 \mu\text{mol L}^{-1}$ and $0.6 \mu\text{mol L}^{-1}$, respectively. In contrast, the
244 near-bottom concentrations of both POC and PN were two times lower, but with comparable POC to PN
245 ratios of 6.1 to 6.2 (Table 1).

246 Near-bottom velocity within the seamount summit area ranged from 0 to $\sim 18 \text{ cm s}^{-1}$, and were on average
247 lower within the coral garden ($\sim 2 \text{ cm s}^{-1}$) than for the non-garden sandy sites ($4 - 7 \text{ cm s}^{-1}$; Table 2). All sites
248 showed tidal influence (e.g., Fig. S1 in the Supplement) superimposed on the local flow dynamics. Based on
249 the flow characteristics (velocity and direction), it was found that the water mass moved slower within the
250 garden than in off-garden regions, thus increasing the theoretical residence time of any particle transported
251 along with the flow (see particle tracks in Fig. S2).

252

253 3.3. Benthic oxygen uptake

254 The aquatic eddy covariance (AEC) system was successfully deployed five times, collecting 126 hours of
255 high-resolution flux data (Table 2). At the coral garden sites, hourly-averaged benthic O₂ uptake rates
256 typically ranged from 4 to 40 mmol m⁻² d⁻¹ (Fig. S1). Each site was characterized by five distinct habitats,
257 i.e., periods with stable flux, with mean O₂ uptake rates in the range of 5 to 40 mmol m⁻² d⁻¹ (see Fig. 3). The
258 mean O₂ uptake rate at the respective coral garden sites, comprising all five habitats, ranged from 10.0 ± 0.8
259 to 18.8 ± 2.0 mmol m⁻² d⁻¹ (mean ± standard error). Mean values for the derived z₀ of the coral garden sites
260 ranged from 6.4 to 7.3 cm, resulting in a theoretical AEC footprint area of 15 to 22 m² with the region of
261 maximum flux (X_{max}) located at a horizontal distance of 0.1 m from the sampling volume (Table S2).

262 In contrast, hourly-averaged benthic O₂ uptake rates at the sandy reference site and the off-garden site
263 ranged from 1 to 12 mmol m⁻² d⁻¹. The mean O₂ uptake at the first sandy reference site was lower, 1.7 ± 0.2
264 mmol m⁻² d⁻¹ (Table 2, Fig. 3), with hourly-averaged rates of up to 4 mmol m⁻² d⁻¹ (Fig. S1). Mean z₀ was
265 reduced to 0.8 cm, resulting in a theoretical AEC footprint of 102 m² (Table S2). At the off-garden sandy
266 site, the O₂ uptake amounted to 7.7 ± 0.8 mmol m⁻² d⁻¹ (Fig. 3), with a mean z₀ of 4.5 cm and an associated
267 theoretical AEC footprint area of 40 m² (Table S2).

268 At the garden sites, O₂ uptake showed little direct correlation with the magnitude of flow velocity or flow
269 direction, though the last deployment (AEC-5) was characterized by narrower range of both velocity and
270 directions (Fig. S3a-c). A more detailed analysis of the uptake vs. flow relation using principal component
271 analysis showed that a large portion of the data variance (58.3%) could be attributed to the local
272 hydrodynamics, i.e., flow velocity and direction (Fig. S3d). However, 35.3% of the variance could only be
273 explained in terms of a second component, which is attributable to habitat characteristics, i.e., faunal density
274 and habitat coverage.

275

276 3.4. Sediment trap

277 Deposition rates of POC, as derived from the sediment trap, covered a period of six months (Table S1).
278 Values varied by a factor of ~20, from 0.077 mmol C m⁻² d⁻¹ during winter to 1.605 mmol C m⁻² d⁻¹ during
279 late spring, being on average 0.454 ± 0.392 mmol C m⁻² d⁻¹ (mean ± sd). Similarly, PN fluxes were the
280 lowest during winter (< 0.020 mmol m⁻² d⁻¹) and up to 0.186 mmol m⁻² d⁻¹ in late spring. The average during
281 the whole observational period was 0.059 ± 0.047 mmol m⁻² d⁻¹. The average ratio of POC to PN was 7.6 ±
282 1.5, which is typical for phytodetritus (see Kiriakoulakis et al. 2009). However, we encountered values as
283 high as 12.6 during winter, implying the deposition of more degraded material, and values of only 5.3 during
284 early spring, which are more typical of phytoplankton at the onset of a spring bloom (Fig. 4, Table S1).

285

286 4. Discussion

287 4.1. Cold-water coral habitats as carbon cycling hotspots.

288 This study provides the first *in situ* estimates of oxygen (O₂) uptake rates for coral gardens. Our results
289 show that the community dominated by *Viminella flagellum* and *Dentomuricea* aff. *meteor* at the summit of
290 Condor seamount represents a hotspot for O₂ uptake. The mean benthic O₂ uptake rate for the coral garden
291 sites (13.5 mmol m⁻² d⁻¹) was more than a factor of two higher than the mean rate observed at the sandy sites,
292 increasing to a factor of ten when considering only the sandy summit reference site (Fig. 3, Table 2). The O₂
293 uptake of 4.6 mmol m⁻² d⁻¹ at the sandy sites is consistent with the global mean benthic *in situ* O₂ uptake
294 rates for other sedimentary habitats at comparable depths (Fig. 3).

295 The O₂ uptake of the coral gardens falls within the lower end of previously published values for CWC
296 habitats (Table 3). While similar rates have been reported for *in situ* incubations of single branches of the
297 reef-building coral *Lophelia pertusa* (Khrifounoff et al. 2014) (Table 3), CWC reef habitats generally appear
298 to have 4 to 10 times higher O₂ consumption rates than the coral gardens at Condor seamount. This
299 presumably reflects that stony CWC framework-forming scleractinians include a rich associated macrofaunal
300 community living on the underlying dead coral framework (coral rubble), which acts as a biocatalytic filter
301 entrapping POM. Coral rubble has been shown to dominate O₂ uptake in such CWC reef communities (e.g.,
302 De Clippele et al. 2021), with average contributions of ~23 mmol m⁻² d⁻¹ (Table 3), while the contributions
303 from live coral patches might be as low as 9% of the total O₂ uptake rate (van Oevelen et al. 2009). It should
304 be noted, however, that the activity of suspension feeders displays a strong seasonality (Rossi et al. 2017)
305 and in oligotrophic systems, such as the Azores, octocoral species have been shown to exhibit lower
306 physiological rates in summer months when productivity is low (Coma et al. 2000, Rossi et al. 2006). The
307 current study took place during the summer, which is marked by low surface productivity (Santos et al.
308 2013) and low POC fluxes (sediment trap data presented herein) and therefore the reported O₂ uptake rates of
309 these communities are likely conservative as annual estimates.

310 Coral gardens primarily develop on consolidated substrates (i.e., fragmented rocks partially covered by
311 depositional sand), with octocoral colonies only covering a small fraction of the available surface (see Fig.
312 1). Our experimental approach did not allow us to assess the contribution of octocorals themselves to the
313 habitat-integrated O₂ uptake rate. However, an approximate estimate was obtained from parallel laboratory-
314 based feeding experiments on the same species collected from Condor seamount (Rakka et al. 2021; Table
315 3). Those experiments determined O₂ respiration rates of $6.24 \pm 4.56 \mu\text{mol g}^{-1} \text{d}^{-1}$ (dry weight) for *V.*
316 *flagellum* and $31.92 \pm 7.68 \mu\text{mol g}^{-1} \text{d}^{-1}$ for *D.* aff. *meteor*, respectively. If we extrapolate the dry weight O₂
317 uptake rates obtained in aquaria to areal rates considering maximum coral densities and average coral sizes
318 measured in Condor summit (where AEC measurements were taken) and convert them to coral biomass, then
319 the contribution from *V. flagellum* and *D.* aff. *meteor* would be 0.45 mmol m⁻² d⁻¹ and 0.06 mmol m⁻² d⁻¹,
320 respectively (~5% of the mean O₂ uptake). This suggests that ~95% of the observed O₂ uptake rate within the

321 coral garden might be attributed to sedimentary respiration and garden-inhabiting fauna rather than corals
322 themselves.

323 Our measurement setup did not allow for a direct comparison of O₂ uptake rates and specific
324 characteristics of the integrated footprint areas (i.e., substrate coverage and faunal density), whose
325 contributions to community O₂ uptake is expected to be well-integrated by the aquatic eddy-covariance
326 technique (see Rovelli et al. 2015, de Froe et al. 2019). As discussed above, coral densities alone cannot
327 account for the enhanced O₂ uptake rates observed across the sites, where the mean habitat O₂ uptake rates
328 varied by up to 8-fold between the lowest and highest values (Fig. 3). Such variation could in part be
329 attributed to differences in proportions of coverage by depositional sand and colonized hard substrate (see
330 Fig. 1, Text S1 in the Supplement) compared to dampened sand deposition and the more colonized hard
331 substrate, as in AEC-2 (see Fig. 1). At the site level, however, community-integrated mean O₂ uptake rates
332 appear to be driven by a complex interplay between habitat characteristics, directly linked to the integrated
333 O₂ uptake, and the local hydrodynamics, which jointly explained most of the data variance (94%; Fig. S3).

334

335 4.2. Supply of organic matter to the coral garden

336 The enhanced carbon cycling of the coral garden implies locally elevated organic matter (OM) supply
337 either through physical processes (i.e., sedimentation and advection) or via an efficient entrapment of OM by
338 the coral communities (e.g., Kiriakoulakis et al. 2004). The hydrodynamic regime at Condor seamount is
339 characterized by a strong anticyclonic Taylor cap, which prevails throughout most of the year, combined
340 with strong tidal mixing and downwelling events over the summit (Bashmachnikov et al., 2013). Although
341 Taylor caps can enhance local productivity by enriching surface waters with nutrients, in the case of Condor
342 Seamount the effect appears to be limited to depths below 170 m, and therefore primary production above
343 the summit is low (Bashmachnikov et al., 2013; Ciancia et al., 2016). However, the anticyclonic circulation
344 causes the retention of organic carbon over the summit, which may provide occasional food pulses that can
345 be utilized and recycled within the coral garden. This is consistent with our particle track analyses (Fig. S2),
346 which showed substantially shortened tracks (i.e., longer residence times) at coral garden sites compared to
347 the sandy sites, indicating that the coral garden is exposed for a longer period of time to any OM transports
348 to the seamount summit when compared to the sandy areas. The supply of particulate OM (POM) to the
349 summit of Condor seamount can be estimated from the sediment trap mooring data. If we assume that all
350 sedimentary POM is respired based on standard Redfield stoichiometry (N:C:O = 16:106:138; Redfield et al.
351 1963) then the combined respiration of particulate organic carbon (POC) and particulate nitrogen (PN)
352 would account for most of the O₂ uptake at the sandy reference sites, but only below 10 % (1.1 mmol m⁻² d⁻¹)
353 of the mean O₂ uptake for the coral gardens. It should be noted, however, that sediment traps can
354 underestimate vertical fluxes, especially in regions with complex topography and hydrodynamics, as
355 advective pathways are often under sampled (e.g., Jahnke et al. 1990). Furthermore, short-time-series

356 measurements (weeks to months) of POC fluxes often miss episodic inputs (Smith et al. 1992). Indirect
357 estimates of the POC supply to the summit from export and subsequent deposition of surface net primary
358 production (NPP), inferred from remote sensing (see <http://sites.science.oregonstate.edu/ocean.productivity>;
359 Behrenfeld & Falkowski 1997) and established export/burial parametrizations (Suess 1980, Dunne et al.
360 2007) also suggest that while local NPP, albeit low, would be sufficient to sustain coral garden habitats
361 during part of the year (e.g., in spring), additional supply pathways would likely be required to do so
362 throughout the year, and especially during summer time (see Fig. S4).

363 Past studies on the OM composition of sediments at Condor seamount showed impoverished OM content
364 of the sediments on the summit compared to its flanks and an off-seamount station (Bongiorni et al. 2013).
365 This was reflected in a lower abundance and biomass of meiofauna in the summit sediments compared to
366 other stations (Zeppilli et al. 2013). Such observations were interpreted to result from the hydrographic
367 conditions on the seamount, where its main currents presumably transport high concentrations of nutrients,
368 plankton and OM, hitting Condor Seamount from the north and then shifting southward, away from the
369 seamount summit and the southern flank (Bashmachnikov et al. 2013, Bongiorni et al. 2013). Thus, it is
370 possible that the considerable amount of available POM that is delivered at depth to the summit area is
371 consumed, or its entrapment facilitated by suspension feeders with little deposition in seafloor sediments.

372 During the study period, chlorophyll *a* (Chl *a*) concentrations were low (Fig. 2), in agreement with
373 previous summer surveys (e.g., Santos et al. 2013) and satellite data (Ciancia et al. 2016), with the lowest
374 values near the bottom (Table 1). Comparable trends were also observed for POM concentrations (Table 1).
375 The low Chl *a* concentration in near-bottom POM could indicate a small contribution of (viable)
376 phytoplankton. The reported mean POC:PN ratio (6.1 ± 1.26) was close to Redfield stoichiometry (6.6)
377 implying that the POM was not significantly degraded. This is in line with the presence of frequent
378 downwelling events over the summit of Condor Seamount (Tempera et al. 2012, Bashmachnikov et al.
379 2013), which may occasionally supply fresh phytoplankton and POM to the coral garden from surface
380 waters. Thus, the O₂ uptake rates observed at the coral garden suggest that these communities efficiently
381 entrap material that sustains high biological activity.

382 The results of this study serve to further validate the strength of the aquatic eddy covariance (AEC)
383 approach to quantify O₂ uptake from CWC habitats, but also highlight the importance that coral gardens may
384 have for local carbon cycling. Given the ubiquitous occurrence of coral gardens, their importance in regional
385 and global biogeochemical cycles should be recognized, especially as changes in the global climate are
386 projected to modify the quantity and quality of the food delivered to deep-sea communities (Sweetman et al.
387 2017, Puerta et al. 2020). The Azores region is projected to experience critical changes in aragonite
388 saturation and POC flux (Puerta et al. 2020), with concomitant predicted reductions of suitable habitats for
389 octocorals (Morato et al. 2020). The baseline information presented here on carbon turnover of coral gardens
390 is essential to understand future changes in the functioning of these important ecosystems.

391 **Acknowledgements**

392 This project has received funding from the European Union’s Horizon 2020 research and innovation
393 programme under grant agreement No 678760 (ATLAS) and grant agreement No 689518 (MERCES).
394 Underwater video images were obtained with funding from the European Community 7th Framework
395 Programme under grant agreement No 213144 (CoralFISH) and grant agreement No 603418 (MIDAS), and
396 Corazon project (FCT/PTDC/MAR/72169/2006) financed by the Fundação para a Ciência e a Tecnologia
397 (FCT). This output reflects only the author’s view and the European Union cannot be held responsible for
398 any use that may be made of the information contained therein. MCS, CD-C, MR, TM also acknowledge
399 funds and support from the FCT through the strategic project (UIDB/05634/2020 and UIDP/05634/2020)
400 granted to OKEANOS and through the FCT Regional Government of the Azores under the project
401 M1.1.A/REEQ.CIENTÍFICO UI&D/2021/010. This study contributes to the project HADES-ERC funded by
402 the European Research Council Advanced Investigator Grant 669947 and to the FNU-7014-00078 grant,
403 awarded by the Danish Council for Independent Research both awarded to RNG. KMA was supported
404 through a Postdoctoral fellowship from the Walter and André de Nottbeck Foundation. LR received funding
405 from the German Science Foundation (grant RO 5921/1-1). CD-C was supported by the PO2020 project
406 DeepWalls (ACORES-01-0145-FEDER-000124) and by the FCT-IP Project UIDP/05634/2020. MR was
407 funded by a DRCT PhD grand grant (reference M3.1.a/F/047/2015.). MCS and TM were supported by
408 Program Stimulus of Scientific Employment (CCCIND/03346/2020 and CCCIND/03345/2020, respectively)
409 from the Fundação para a Ciência e Tecnologia. We thank António Godinho and the crew of the R/V *Águas*
410 *Vivas* for their substantial support during the field activities and the scientific team involved in the collection
411 of underwater video images. We are also thankful to Anni Glud and Rikke Orloff Holm for their support in
412 the nutrients analyses.

413

414
415
416
417
418
419
420
421
422
423
424
425
426
427
428
429
430
431
432
433
434
435
436
437
438
439
440
441
442
443
444
445
446
447
448
449
450
451
452
453
454
455
456
457
458
459
460
461
462
463
464
465
466

References

- Attard KM, Glud RN, McGinnis DF, Rysgaard S (2014) Seasonal rates of benthic primary production in a Greenland fjord measured by aquatic eddy correlation. *Limnol Oceanogr* 59:1555–1569.
- Bashmachnikov I, Loureiro CM, Martins A (2013) Topographically induced circulation patterns and mixing over Condor seamount. *Deep Sea Res Part II Top Stud Oceanogr* 98:38–51.
- Behrenfeld MJ, Falkowski PG (1997) Photosynthetic rates derived from satellite-based chlorophyll concentration. *Limnol Oceanogr* 42:1–20.
- Berg P, Delgard ML, Polsenaere P, McGlathery KJ, Doney SC, Berger AC (2019) Dynamics of benthic metabolism, O₂, and pCO₂ in a temperate seagrass meadow. *Limnol Oceanogr* 64:2586–2604.
- Berg P, Roy H, Wiberg PL (2007) Eddy correlation flux measurements: The sediment surface area that contributes to the flux. *Limnol Oceanogr* 52:1672–1684.
- Bongiorni L, Ravara A, Parretti P, Santos RS, Rodrigues CF, Amaro T, Cunha MR (2013) Organic matter composition and macrofaunal diversity in sediments of the Condor Seamount (Azores, NE Atlantic). *Deep Sea Res Part II Top Stud Oceanogr* 98:75–86.
- Buhl-Mortensen L, Buhl-Mortensen P (2018) Cold Temperate Coral Habitats. In: *Corals in a Changing World*. Beltran CD, Camacho ET (eds) InTech, London
- Buhl-Mortensen L, Serigstad B, Buhl-Mortensen P, Olsen MN, Ostrowski M, Błażewicz-Paszkwyc M, Appoh E (2017) First observations of the structure and megafaunal community of a large *Lophelia* reef on the Ghanaian shelf (the Gulf of Guinea). *Deep Sea Res Part II Top Stud Oceanogr* 137:148–156.
- Buhl-Mortensen L, Vanreusel A, Gooday AJ, Levin LA, Priede IG, Buhl-Mortensen P, Gheerardyn H, King NJ, Raes M (2010) Biological structures as a source of habitat heterogeneity and biodiversity on the deep ocean margins. *Mar Ecol* 31:21–50.
- Carmo V, Santos M, Menezes GM, Loureiro CM, Lambardi P, Martins A (2013) Variability of zooplankton communities at Condor seamount and surrounding areas, Azores (NE Atlantic). *Deep Sea Res Part II Top Stud Oceanogr* 98:63–74.
- Carreiro-Silva M, Ocaña O, Stanković D, Sampaio Í, Porteiro FM, Fabri M-C, Stefanni S (2017) Zoantharians (Hexacorallia: Zoantharia) Associated with Cold-Water Corals in the Azores Region: New Species and Associations in the Deep Sea. *Front Mar Sci* 4:88.
- Cathalot C, Van Oevelen D, Cox TJS, Kutti T, Lavaleye M, Duineveld G, Meysman FJR (2015) Cold-water coral reefs and adjacent sponge grounds: hotspots of benthic respiration and organic carbon cycling in the deep sea. *Front Mar Sci* 2:1–12.
- Ciancia E, Magalhães Loureiro C, Mendonça A, Coviello I, Di Polito C, Lacava T, Pergola N, Satriano V, Tramutoli V, Martins A (2016) On the potential of an RST-based analysis of the MODIS-derived chl-a product over Condor seamount and surrounding areas (Azores, NE Atlantic). *Ocean Dyn* 66:1165–1180.
- De Clippele LH, Rovelli L, Ramiro-Sánchez B, Kazanidis G, Vad J, Turner S, Glud RN, Roberts JM (2021) Mapping cold-water coral biomass: an approach to derive ecosystem functions. *Coral Reefs* 40:215–231.
- Coma R, Ribes M, Gili J-M, Zabala M (2000) Seasonality in coastal benthic ecosystems. *Trends Ecol Evol* 15:448–453.
- Coppari M, Zanella C, Rossi S (2019) The importance of coastal gorgonians in the blue carbon budget. *Sci Rep* 9:13550.
- Davies AJ, Guinotte JM (2011) Global Habitat Suitability for Framework-Forming Cold-Water Corals. *PLoS One* 6:e18483.
- Dodds LA, Roberts JM, Taylor AC, Marubini F (2007) Metabolic tolerance of the cold-water coral *Lophelia pertusa* (Scleractinia) to temperature and dissolved oxygen change. *J Exp Mar Bio Ecol* 349:205–214.
- Dunne JP, Sarmiento JL, Gnanadesikan A (2007) A synthesis of global particle export from the surface ocean and cycling through the ocean interior and on the seafloor. *Global Biogeochem Cycles* 21:Gb4006.
- de Froe E, Rovelli L, Glud RN, Maier SR, Duineveld G, Mienis F, Lavaleye M, van Oevelen D (2019) Benthic Oxygen and Nitrogen Exchange on a Cold-Water Coral Reef in the North-East Atlantic Ocean. *Front Mar Sci* 6:665.

- 467 Glud RN (2008) Oxygen dynamics of marine sediments. *Mar Biol Res* 4:243–289.
- 468 Gomes-Pereira JN, Carmo V, Catarino D, Jakobsen J, Alvarez H, Aguilar R, Hart J, Giacomello E, Menezes
469 G, Stefanni S, Colaço A, Morato T, Santos RS, Tempera F, Porteiro F (2017) Cold-water corals and
470 large hydrozoans provide essential fish habitat for *Lappanella fasciata* and *Benthocometes robustus*.
471 *Deep Sea Res Part II Top Stud Oceanogr* 145:33–48.
- 472 Goring DG, Nikora VI (2002) Despiking acoustic Doppler velocimeter data. *J Hydraul Eng* 128:117–126.
- 473 Henry L-A, Roberts JM (2017) Global Biodiversity in Cold-Water Coral Reef Ecosystems. In: *Marine
474 Animal Forests*. Springer International Publishing, Cham, p 235–256
- 475 Holm-Hansen O, Lorenzen CJ, Holmes RW, Strickland JDH (1965) Fluorometric Determination of
476 Chlorophyll. *ICES J Mar Sci* 30:3–15.
- 477 Huettel M, Berg P, Merikhi A (2020) Technical note: Measurements and data analysis of sediment–water
478 oxygen flux using a new dual-optode eddy covariance instrument. *Biogeosciences* 17:4459–4476.
- 479 Inoue T, Glud RN, Stahl H, Hume A (2011) Comparison of three different methods for assessing in situ
480 friction velocity: A case study from Loch Etive, Scotland. *Limnol Oceanogr* 9:275–287.
- 481 Jahnke RA, Reimers C., Craven DB (1990) Intensification of recycling of organic matter at the sea floor near
482 ocean margins. *Nature* 348:50–54.
- 483 Khripounoff A, Caprais J, Le Bruchec J, Rodier P, Noel P, Cathalot C (2014) Deep cold-water coral
484 ecosystems in the Brittany submarine canyons (Northeast Atlantic): Hydrodynamics, particle supply,
485 respiration, and carbon cycling. *Limnol Oceanogr* 59:87–98.
- 486 Kiriakoulakis K, Bett BJ, White M, Wolff GA (2004) Organic biogeochemistry of the Darwin Mounds, a
487 deep-water coral ecosystem, of the NE Atlantic. *Deep Sea Res Part I Oceanogr Res Pap* 51:1937–1954.
- 488 Kiriakoulakis K, Vilas JC, Blackbird SJ, Arístegui J, Wolff GA (2009) Seamounts and organic matter—Is
489 there an effect? The case of Sedlo and Seine seamounts, Part 2. Composition of suspended particulate
490 organic matter. *Deep Sea Res Part II Top Stud Oceanogr* 56:2631–2645.
- 491 Lampitt R., Bett B., Kiriakoulakis K, Popova E., Ragueneau O, Vangriesheim A, Wolff G. (2001) Material
492 supply to the abyssal seafloor in the Northeast Atlantic. *Prog Oceanogr* 50:27–63.
- 493 Long MH, Berg P, de Beer D, Ziemann JC (2013) In Situ Coral Reef Oxygen Metabolism: An Eddy
494 Correlation Study. *PLoS One* 8:e58581.
- 495 Lorke A, McGinnis DF, Maeck A (2013) Eddy-correlation measurements of benthic fluxes under complex
496 flow conditions: Effects of coordinate transformations and averaging time scales. *Limnol Oceanogr*
497 11:425–437.
- 498 McGinnis DF, Cherednichenko S, Sommer S, Berg P, Rovelli L, Schwarz R, Glud RN, Linke P (2011)
499 Simple, robust eddy correlation amplifier for aquatic dissolved oxygen and hydrogen sulfide flux
500 measurements. *Limnol Oceanogr* 9:340–347.
- 501 McGinnis DF, Sommer S, Lorke A, Glud RN, Linke P (2014) Quantifying tidally driven benthic oxygen
502 exchange across permeable sediments: An aquatic eddy correlation study. *J Geophys Res Ocean*
503 119:6918–6932.
- 504 Morato T, González-Irusta J, Dominguez-Carrió C, Wei C, Davies A, Sweetman AK, Taranto GH, Beazley
505 L, García-Alegre A, Grehan A, Laffargue P, Murillo FJ, Sacau M, Vaz S, Kenchington E, Arnaud-
506 Haond S, Callery O, Chimienti G, Cordes E, Egilsdottir H, Freiwald A, Gasbarro R, Gutiérrez-Zárate
507 C, Gianni M, Gilkinson K, Wareham Hayes VE, Hebbeln D, Hedges K, Henry L, Johnson D, Koen-
508 Alonso M, Lirette C, Mastrototaro F, Menot L, Molodtsova T, Durán Muñoz P, Orejas C, Pennino MG,
509 Puerta P, Ragnarsson SÁ, Ramiro-Sánchez B, Rice J, Rivera J, Roberts JM, Ross SW, Rueda JL,
510 Sampaio Í, Snelgrove P, Stirling D, Treble MA, Urrea J, Vad J, Oevelen D, Watling L, Walkusz W,
511 Wienberg C, Woillez M, Levin LA, Carreiro-Silva M (2020) Climate-induced changes in the suitable
512 habitat of cold-water corals and commercially important deep-sea fishes in the North Atlantic. *Glob
513 Chang Biol* 26:2181–2202.
- 514 van Oevelen D, Duineveld G, Lavaleye M, Mienis F, Soetaert K, Heip CHR (2009) The cold-water coral
515 community as a hot spot for carbon cycling on continental margins: A food-web analysis from Rockall
516 Bank (northeast Atlantic). *Limnol Oceanogr* 54:1829–1844.
- 517 Pham CK, Gomes-Pereira JN, Isidro EJ, Santos RS, Morato T (2013) Abundance of litter on Condor
518 seamount (Azores, Portugal, Northeast Atlantic). *Deep Sea Res Part II Top Stud Oceanogr* 98:204–208.
- 519 Porteiro FM, Gomes-Pereira JN, Pham CK, Tempera F, Santos RS (2013) Distribution and habitat

520 association of benthic fish on the Condor seamount (NE Atlantic, Azores) from in situ observations.
521 Deep Sea Res Part II Top Stud Oceanogr 98:114–128.

522 Puerta P, Johnson C, Carreiro-Silva M, Henry L-A, Kenchington E, Morato T, Kazanidis G, Rueda JL, Urra
523 J, Ross S, Wei C-L, González-Irusta JM, Arnaud-Haond S, Orejas C (2020) Influence of Water Masses
524 on the Biodiversity and Biogeography of Deep-Sea Benthic Ecosystems in the North Atlantic. Front
525 Mar Sci 7:239.

526 Rakka M, Maier SR, Van Oevelen D, Godinho A, Bilan M, Orejas C, Carreiro-Silva M (2021) Contrasting
527 metabolic strategies of two co-occurring deep-sea octocorals. Sci Rep 11:10633.

528 Redfield AC, Ketchum BH, Richards FA (1963) The Influence of Organisms on the Composition of the Sea
529 Water. In: *The Sea*, Vol. 2. Hill MN (ed) Interscience Publisher, New York, p 26–77

530 Reidenbach MA, Berg P, Hume A, Hansen JCR, Whitman ER (2013) Hydrodynamics of intertidal oyster
531 reefs: The influence of boundary layer flow processes on sediment and oxygen exchange. Limnol
532 Oceanogr Fluids Environ 3:225–239.

533 Roberts JM, Davies AJ, Henry LA, Dodds LA, Duineveld GCA, Lavaleye MSS, Maier C, van Soest R,
534 Bergman M, Hühnerbach V, Huvenne VAI, Sinclair DJ, Watmough T, Long D, Green SL, van Haren
535 H (2009) Mingulay reef complex: an interdisciplinary study of cold-water coral habitat, hydrography
536 and biodiversity. Mar Ecol Prog Ser 397:139–151.

537 Roberts JM, Wheeler AJ, Freiwald A (2006) Reefs of the deep: The biology and geology of cold-water coral
538 ecosystems. Science (80-) 312:543–547.

539 Rodil IF, Attard KM, Norkko J, Glud RN, Norkko A (2019) Towards a sampling design for characterizing
540 habitat-specific benthic biodiversity related to oxygen flux dynamics using Aquatic Eddy Covariance.
541 PLoS One 14:e0211673.

542 Rossi S, Bramanti L, Gori A, Orejas C (eds) (2017) Marine Animal Forests. The Ecology of Benthic
543 Biodiversity Hotspots. Springer International Publishing, Cham.

544 Rossi S, Gili J-M, Coma R, Linares C, Gori A, Vert N (2006) Temporal variation in protein, carbohydrate,
545 and lipid concentrations in *Paramuricea clavata* (Anthozoa, Octocorallia): evidence for summer–
546 autumn feeding constraints. Mar Biol 149:643–651.

547 Rovelli L, Attard KM, Bryant LD, Flögel S, Stahl H, Roberts JM, Linke P, Glud RN (2015) Benthic O₂
548 uptake of two cold-water coral communities estimated with the non-invasive eddy correlation
549 technique. Mar Ecol Prog Ser 525:97–104.

550 Rovelli L, Attard KM, Cárdenas CA, Glud RN (2019) Benthic primary production and respiration of shallow
551 rocky habitats: a case study from South Bay (Doumer Island, Western Antarctic Peninsula). Polar Biol
552 42:1459–1474.

553 Santos M, Moita MT, Bashmachnikov I, Menezes GM, Carmo V, Loureiro CM, Mendonça A, Silva AF,
554 Martins A (2013) Phytoplankton variability and oceanographic conditions at Condor seamount, Azores
555 (NE Atlantic). Deep Sea Res Part II Top Stud Oceanogr 98:52–62.

556 Smith KL, Baldwin RJ, Williams PM (1992) Reconciling particulate organic carbon flux and sediment
557 community oxygen consumption in the deep North Pacific. Nature 359:313–316.

558 Suess E (1980) Particulate Organic-Carbon Flux in the Oceans - Surface Productivity and Oxygen
559 Utilization. Nature 288:260–263.

560 Sweetman AK, Thurber AR, Smith CR, Levin LA, Mora C, Wei C-L, Gooday AJ, Jones DOB, Rex M,
561 Yasuhara M, Ingels J, Ruhl HA, Frieder CA, Danovaro R, Würzberg L, Baco A, Grupe BM, Pasulka A,
562 Meyer KS, Dunlop KM, Henry L-A, Roberts JM (2017) Major impacts of climate change on deep-sea
563 benthic ecosystems. Elem Sci Anthr 5:4.

564 Tempera F, Giacomello E, Mitchell NC, Campos AS, Braga Henriques A, Bashmachnikov I, Martins A,
565 Mendonça A, Morato T, Colaço A, Porteiro FM, Catarino D, Gonçalves J, Pinho MR, Isidro EJ, Santos
566 RS, Menezes G (2012) Mapping Condor Seamount Seafloor Environment and Associated Biological
567 Assemblages (Azores, NE Atlantic). In: *Seafloor Geomorphology as Benthic Habitat*. Elsevier, p 807–
568 818

569 Tempera F, Hipólito A, Madeira J, Vieira S, Campos AS, Mitchell NC (2013) Condor seamount (Azores, NE
570 Atlantic): A morpho-tectonic interpretation. Deep Res Part II Top Stud Oceanogr 98:7–23.

571 White M, Bashmachnikov I, Arstegui J, Martins A (2008) Physical Processes and Seamount Productivity. In:
572 *Seamounts: Ecology, Fisheries & Conservation*. Blackwell Publishing Ltd, Oxford, UK, p 62–84

- 573 White M, Wolff G, Lundälv T, Guihen D, Kiriakoulakis K, Lavaleye M, Duineveld G (2012) Cold-water
574 coral ecosystem (Tisler Reef, Norwegian Shelf) may be a hotspot for carbon cycling. *Mar Ecol Prog*
575 *Ser* 465:11–23.
- 576 Yamamuro M, Kayanne H (1995) Rapid direct determination of organic carbon and nitrogen in carbonate-
577 bearing sediments with a Yanaco MT-5 CHN analyzer. *Limnol Oceanogr* 40:1001–1005.
- 578 Yesson C, Taylor ML, Tittensor DP, Davies AJ, Guinotte J, Baco A, Black J, Hall-Spencer JM, Rogers AD
579 (2012) Global habitat suitability of cold-water octocorals. *J Biogeogr* 39:1278–1292.
- 580 Zeppilli D, Bongiorno L, Cattaneo A, Danovaro R, Santos RS (2013) Meiofauna assemblages of the Condor
581 Seamount (North-East Atlantic Ocean) and adjacent deep-sea sediments. *Deep Sea Res Part II Top*
582 *Stud Oceanogr* 98:87–100.
- 583

584
585
586
587
588

Tables

Table 1. Overview of baseline temperature, Chlorophyll a, nutrients and POM data at the deep Chlorophyll a maximum and near-bottom at the Condor Seamount. Mean temperature and concentrations of nitrate (NO_3^-), nitrite (NO_2^-), ammonium (NH_4^+), ortho phosphate (PO_4^{3-}), particulate nitrogen (PN), particulate organic carbon (POC) and particulate inorganic carbon (PIC) are presented as mean \pm standard deviation.

Parameter	Chlorophyll a maximum 60 \pm 8 m depth	Near-bottom water 203 \pm 5 m depth
Temperature ($^\circ\text{C}$)	17.0 \pm 0.4	14.9 \pm 0.2
Chlorophyll a ($\mu\text{g L}^{-1}$)	0.84 \pm 0.30	0.04 \pm 0.02
NO_3^- ^a ($\mu\text{mol L}^{-1}$)	1.1 \pm 1.0	6.0 \pm 0.9
NO_2^- ^b ($\mu\text{mol L}^{-1}$)	b. d.	b. d.
NH_4^+ ^b ($\mu\text{mol L}^{-1}$)	0.6 \pm 0.6	b. d.
PO_4^{3-} ($\mu\text{mol L}^{-1}$)	0.1 \pm 0.06	0.4 \pm 0.05
PN ($\mu\text{mol L}^{-1}$)	0.45 \pm 0.11	0.25 \pm 0.08
PC ($\mu\text{mol L}^{-1}$)	3.73 \pm 0.62	1.66 \pm 0.93
POC ($\mu\text{mol L}^{-1}$)	3.56 \pm 0.68	1.55 \pm 0.69
PIC ($\mu\text{mol L}^{-1}$)	0.17 \pm 0.12	0.14 \pm 0.27
POC / PN	6.23 \pm 0.67	6.10 \pm 1.26

589
590

a: from total NO_3^- and NO_2^- minus NO_2^- .

b: Mean values were below detection (b. d.; $<0.1 \mu\text{mol L}^{-1}$)

591 Table 2. Overview of aquatic eddy covariance (AEC) deployments combined with physicochemical parameters, flow velocity magnitude, dissolved
 592 oxygen (O₂) concentration and benthic O₂ uptake rates. Values for the respective parameters are reported as mean ± standard deviation and as a range
 593 within brackets. Mean O₂ fluxes are presented as mean ± standard error.

Site	AEC	Coordinates	Date	Depth	Duration	Temperature	Salinity	Velocity	O ₂	O ₂	O ₂ uptake
	Depl.		(Depl./Retr.)	(m)	(h) ^a	(°C)		(cm s ⁻¹)	(% saturation)	(μmol L ⁻¹)	(mmol m ⁻² d ⁻¹)
Sand	AEC-1	38° 32.7249' N	11 Jul 2018	210	19.0	14.5 ± 0.1	36.0 ± 0.02	4.4 ± 2.2	89.2 ± 0.7	221.8 ± 1.3	1.7 ± 0.1
		29° 03.2079' W	12 Jul 2018		[22.0]	[14.3 – 14.8]	[35.97 – 36.05]	[0 – 13.0]	[87.9 – 91.2]	[219.3 – 225.2]	
Sand (off garden)	AEC-4	38° 32.4221' N	21 Jul 2018	205	19.3	14.9 ± 0.3	36.1 ± 0.04	6.9 ± 3.8	92.7 ± 0.7	228.4 ± 2.0	7.5 ± 0.6
		29° 02.2967' W	23 Jul 2018		[46.2]	[14.5 – 15.6]	[36.01 – 36.13]	[0 – 17.7]	[91.4 – 94.2]	[223.6 – 232.0]	
Coral garden	AEC-2	38° 32.3813' N	16 Jul 2018	203	20	14.7 ± 0.2	36.0 ± 0.03	1.8 ± 1.1	91.9 ± 0.9	227.4 ± 2.4	18.8 ± 2.0
		29° 02.3493' W	17 Jul 2018		[20.9]	[14.4 – 15.1]	[35.96 – 36.10]	[0 – 5.5]	[89.8 – 94.3]	[223.1 – 234.3]	
Coral garden	AEC-3	38° 32.3953' N	17 Jul 2018	206	42.0	14.8 ± 0.2	36.1 ± 0.03	1.9 ± 1.0	91.8 ± 0.8	226.5 ± 1.2	10.0 ± 0.8
		29° 02.3311' W	20 Jul 2018		[68.0]	[14.3 – 15.2]	[35.98 – 36.12]	[0 – 6.1]	[89.5 – 95.0]	[223.1 – 235.2]	
Coral garden	AEC-5	38° 32.3710' N	24 Jul 2018	204	25.3	14.7 ± 0.1	36.0 ± 0.02	2.2 ± 1.1	93.6 ± 0.8	231.7 ± 2.3	11.5 ± 0.5
		29° 02.3362' W	01 Aug 2018		[189.6]	[14.4 – 15.0]	[36.00 – 36.08]	[0 – 6.1]	[92.3 – 96.1]	[228.1 – 237.1]	

a: Number of hours used for O₂ flux calculations. The total duration of the AEC deployment is given in parenthesis.

594
595

596 Table 3. Overview of literature oxygen uptake (in $\text{mmol m}^{-2} \text{d}^{-1} \pm$ standard error [number of replicates]) by cold-water coral communities and from isolated
 597 coral specimens. Note that carbon-based uptake rates were converted to O_2 assuming a 1:1 ratio (see Glud 2008).

Site <i>Location</i>	Depth (m)	O_2 uptake rate ($\text{mmol m}^{-2} \text{d}^{-1}$) [n]	Global ^a	Method ^b	Description	Reference
Condor seamount <i>Azores, Portugal</i>	204	13.4 [3] ^c	5.5	AEC	Coral garden	this study
Haas mound <i>Rockall Bank, NE-Atlantic</i>	536	17.0 [2] ^d	2.7	AEC	Coral rubble community	de Froe et al. (2019)
Oreo mound <i>Rockall Bank, NE-Atlantic</i>	745	45.3 \pm 11.7 [1]	2.1	AEC	Coral rubble & live <i>Lophelia</i> patches	de Froe et al. (2019)
Mingulay Reef Complex <i>Hebrides Sea, off Scotland</i>	128	27.8 \pm 2.3 [1]	7.8	AEC	Coral rubble community	Rovelli et al. (2015)
Stjernsund <i>Northern Norway</i>	220	24.8 \pm 2.6 [1]	5.2	AEC	Coral rubble community	Rovelli et al. (2015)
Træna Marine Protected Area <i>continental shelf of Norway</i>	294	121.5 \pm 9.9 ^e [2]	4.2	AEC	Live CWC reef	Cathalot et al. (2015)
Træna Marine Protected Area <i>continental shelf of Norway</i>	280	81.7 \pm 9.8 [1]	4.2	ICis	Estimated via upscaling	Cathalot et al. (2015)
Tisler Reef <i>Northern Skagerak, Norway</i>	122	40.0 [8]	8.1	OW	Live <i>L. pertusa</i> on coral framework	White et al. (2012)
Guilvinec & Croisic canyon <i>Brittany, NE-Atlantic</i>	850 – 880	7.7 [n.a. ^f]	1.9	ICis	Branch of <i>L. pertusa</i> or <i>M. oculata</i> (3 branches m^{-2})	Khripounoff et al. (2014)
Condor seamount <i>Azores, Portugal</i>	200 – 270	0.07	3.1 – 5.6	ICes	<i>Viminella flagellum</i>	Rakka et al. (2021)
Cap de creus <i>Catalunya, Spain</i>	200 – 270 35 – 70	0.02 0.005 \pm 0.005	3.1 – 5.6 12.2 – 20.4	ICes OW	<i>Dentomuricea</i> aff. <i>meteor</i> <i>Paramuricea clavata</i> gardens	Rakka et al. (2021) Coppari et al.(2019)
Rockall Bank, <i>NE-Atlantic</i>	294	54.4 \pm 4.7 ^e [2]	2.0	AEC	Sponge ground	Cathalot et al. (2015)

598 a: Global mean O_2 uptake for sedimentary habitats at comparable water depths, after Glud (2008).

599 b: Methods include aquatic eddy covariance (AEC), open water budget (OW), incubations *in situ* (ICis), incubations *ex situ* (ICes), and model-based upscaling (M).

600 c: Mean from three sites (10.0 ± 0.8 , 11.5 ± 0.5 , $18.8 \pm 2.0 \text{ mmol m}^{-2} \text{d}^{-1}$, respectively, Table 2).

601 d: Mean from two habitats (22.4 ± 5.6 and $11.5 \pm 3.6 \text{ mmol m}^{-2} \text{d}^{-1}$, respectively).

602 e: mean \pm standard deviation.

603 f: not available

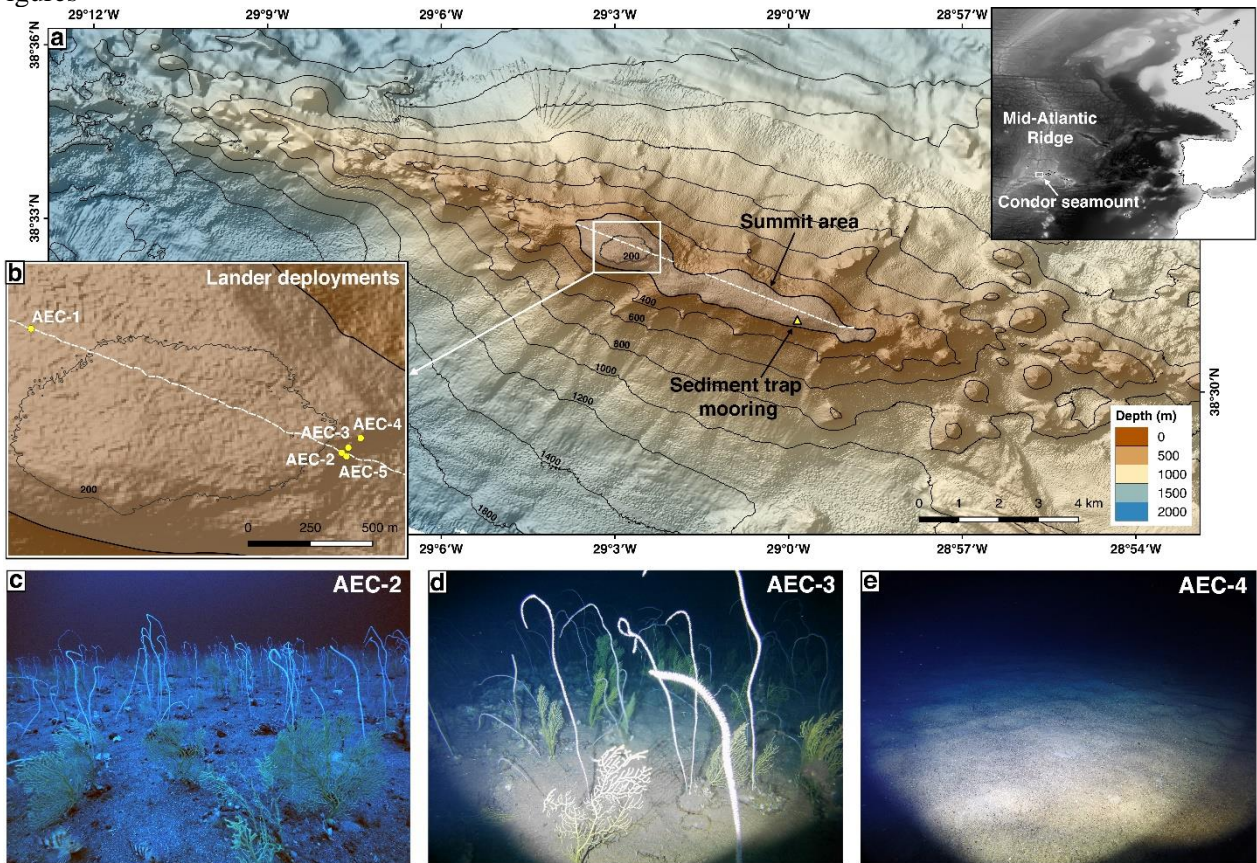


Figure 1. Case study site. (a) Map of Condor seamount (SW Faial island, Azores) displaying the location of the sediment trap mooring (white triangle) and the path of the Hopper towed camera system over the summit (white dashed line), which was used to select suitable areas for aquatic eddy covariance (AEC) deployments. (b) Path of the towed camera system (white striped line) and location of the five AEC deployments on the shallowest part of the summit (coordinates of each deployment provided in Table 2). (c-d) Examples of the images taken with the cameras mounted on the AEC frame showing a dense coral garden formed by the whip octocoral *Viminella flagellum* and the fan-shaped octocoral *Dentomuricea* aff. *meteor*. (e) Image taken from the AEC frame in the sandy area located just a few meters off the coral garden site.

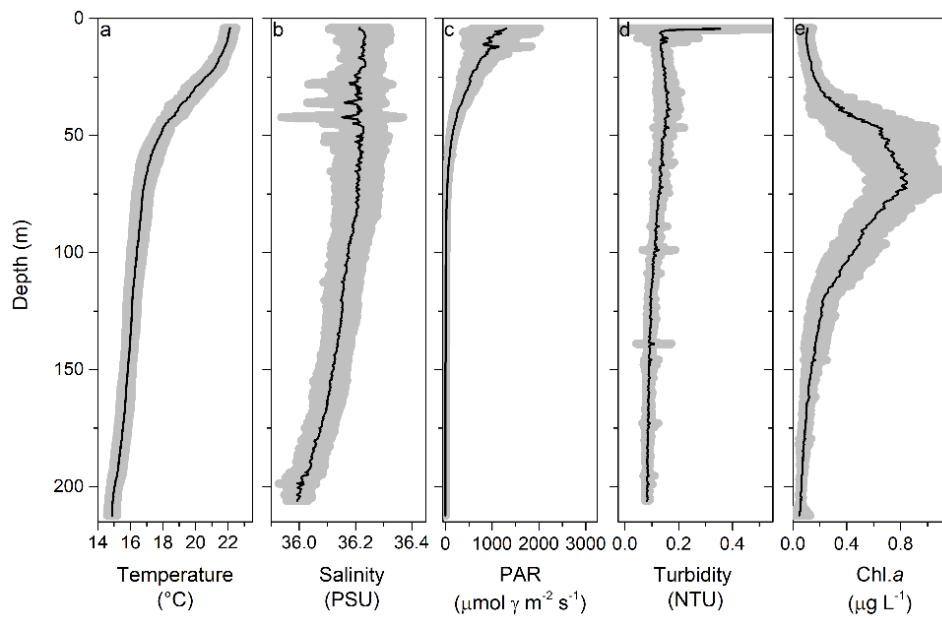


Figure 2. Mean water column profiles for temperature (a), salinity (b), photosynthetically active radiation (PAR; c), turbidity (d) and chlorophyll *a* (Chl. *a*; e) based on all collected casts (n=36). The shaded area represents the standard deviation.

606

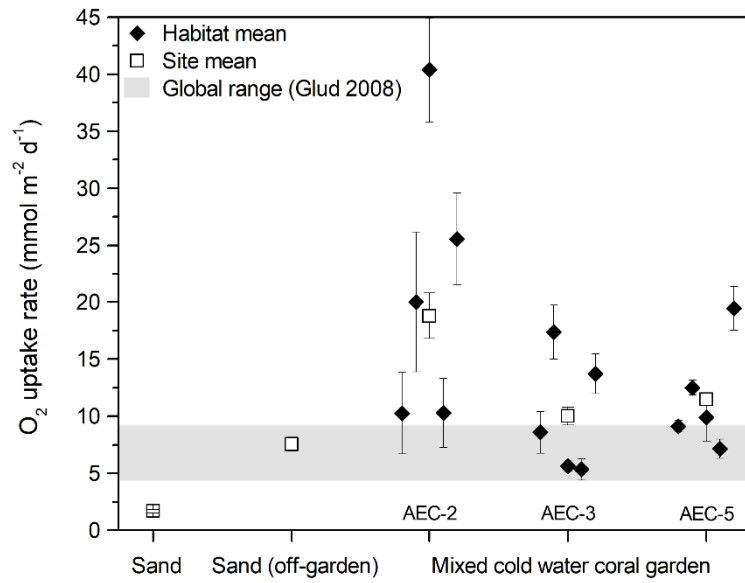


Figure 3. Overview of all O₂ uptake rates from the mixed cold water coral garden and sandy sites (Table 2) from our aquatic eddy covariance deployments. Error bars indicate the standard error for habitat means and standard deviation for site means. Global range of *in situ* O₂ uptake rates for sedimentary habitats at comparable water depths (175 – 266 m) is reported after Glud (2008).

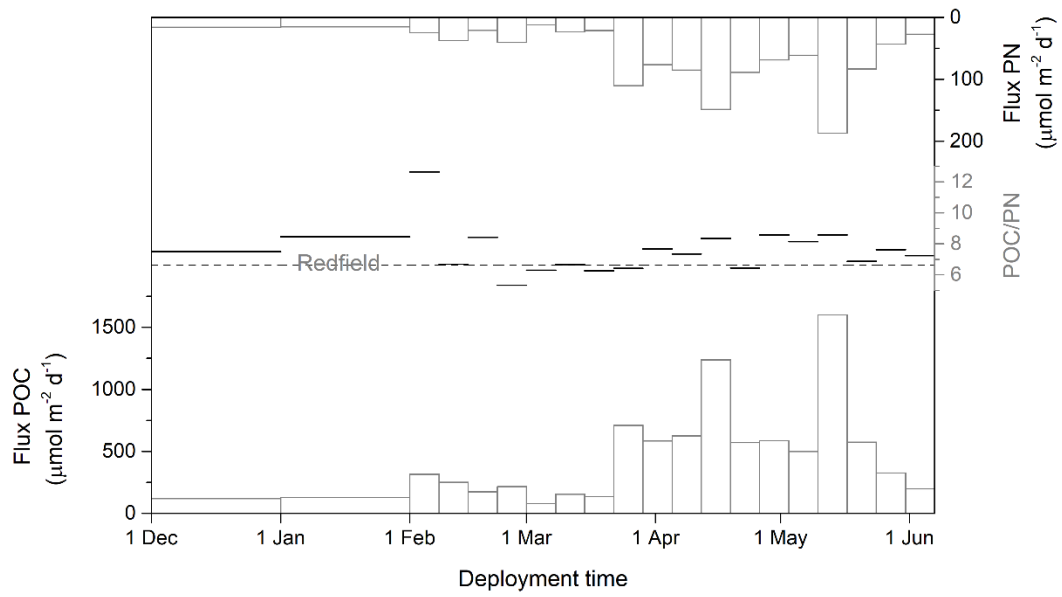


Figure 4. Fluxes of particulate organic carbon (POC; bottom) and particulate nitrogen (PN; top) from our long-term sediment trap mooring (see Table S1 in the Supplement). The POC to PN ratio for each sampling period (center) is provided with the Redfield ratio (6.325) for intercomparisons.

608

Electronic Supplement for

Benthic O₂ uptake by coral gardens at the Condor seamount (Azores)

Lorenzo Rovelli^{1,8*}, Marina Carreiro-Silva^{2,3}, Karl M. Attard^{1,4,5}, Maria Rakka^{2,3}, Carlos Dominguez-Carrió^{2,3}, Meri Bilan^{2,3}, Sabena Blackbird⁶, Telmo Morato^{2,3}, George A. Wolff⁶, Ronnie N. Glud^{1,5,7}

¹HADAL & Nordcee, Department of Biology, University of Southern Denmark, 5230 Odense M, Denmark

²IMAR – Instituto do Mar, Universidade dos Açores, 9901-862 Horta, Portugal

³Instituto de Investigação em Ciências do Mar – Okeanos, Universidade dos Açores, 9901-862 Horta, Portugal

⁴Tvärminne Zoological Station, University of Helsinki, 10900 Hanko, Finland

⁵Danish Institute of Advanced Study – DIAS, University of Southern Denmark, 5230 Odense M, Denmark

⁶School of Environmental Sciences, University of Liverpool, L69 3GP Liverpool, United Kingdom

⁷Department of Ocean and Environmental Sciences, Tokyo University of Marine Science and Technology, 108-8477 Tokyo, Japan

⁸now at iES – Institute for Environmental Sciences, University of Koblenz-Landau, 76829 Landau, Germany

*corresponding author

Content: 1 Text, 2 Tables, 4 Figures

This document contains additional information on the sediment trap data, processing of the aquatic eddy covariance (AEC) dataset, analysis of the local hydrodynamics and relationship between AEC-based fluxes and flow velocity and direction. Text S1 provides a more detailed description of the correlation between oxygen (O_2) uptake and flow characteristics (magnitude and direction) depicted in Figure S3. Table S1 presents an overview of the data obtained from the sediment trap deployments as shown in Figure 4. Table S2 provides the mean characteristics of the theoretical AEC footprint area integrated by AEC measurements at the respective sites. Figure S1 shows examples of the AEC dataset for a coral garden site and the reference sandy site, and provides a visual depiction of the procedure used to identify periods of stable flux (i.e., habitats) for the garden sites as described in the Methods section. Figure S2 shows the theoretical particle track analysis for each site. Figure S3 shows the flow velocity, flow direction and O_2 uptake correlation plots for the garden sites together with the associated principal component analysis, as detailed in Text S1. Figure S4 shows local estimates of net primary production based on remote sensing and the associated flux of particulate organic carbon (POC) based on established empirical relationships (see Figure S4 caption for details).

Text S1. Coral garden site characterization from oxygen (O₂) uptake and flow characteristics

Within the coral garden sites, mean habitat O₂ uptake rates ranged from 5 to 40 mmol m⁻² d⁻¹ (Fig. 3). Compared with the global range from sedimentary habitats at similar depths (after Glud 2008), the mean habitats rates reported for AEC-2 were systematically higher, up to a factor of 4. In contrast, for AEC-3 and AEC-5, the habitats' mean uptake fell closer to the rates observed across the sandy sites, with only 2-3 habitats showing enhanced O₂ uptake rates (Fig. 3). This could be in part explained by the presence of habitats with different proportions of depositional sand and more colonized hard substrates, both across sites and within sites. While our experimental setup did not allow for a direct quantification of faunal densities and proportion of colonized areas, our benthic imaging (e.g., Fig. 1) hints at larger proportion of depositional sand at AEC-3 and AEC-5 than at AEC-2, in agreement with the observed differences in O₂ uptake (Fig. 3).

The local hydrodynamics regime was also found to modulate the observed O₂ uptake dynamics. In fact, in our principal component analysis (PCA), flow velocity and direction alone, when expressed as principal component 1, explained almost 60% of the data variance, contrasting with the ~35% of the second principal component, which was clearly identifiable as being driven by habitats-specific faunal density and habitat coverage. (Fig. 3d). Based on flow characteristics, all three sites showed a comparable flow velocity range, but AEC-2 and AEC-3 were characterized by slightly lower mean flow velocities than AEC-5 (Table 2), as also depicted visually by the site-specific particle tracks (see Fig. S2). It is thus not surprising that in the PCA, AEC-2 and AEC-3 are clustered together and spread along the second principal component while AEC-5 is clearly separated from the other two sites. It should be noted that the actual location of the sites within the summit varied very little, by less than 50 m (Fig. 1), suggesting that the differences in flow velocities and direction (see Fig. S2) may be in part due to the integration between the flow and localized small-scale topography features. Overall, our PCA, albeit limited by the reduced amount of available measurements, suggests that the benthic O₂ uptake is ultimately driven by a complex interplay between the local hydrodynamics and habitat characteristics, i.e., faunal density and habitat coverage.

Table S1. Overview of sediment trap sampling showing the integrated fluxes of particulate nitrogen (PN) and carbon (PC), particulate organic carbon (POC), particulate inorganic carbon (PIC) as well as the POC to PN ratio.

Bottle number	Opening date	Closing date	Days	PN ($\mu\text{mol m}^{-2} \text{d}^{-1}$)	PC ($\mu\text{mol m}^{-2} \text{d}^{-1}$)	POC ($\mu\text{mol m}^{-2} \text{d}^{-1}$)	PIC ($\mu\text{mol m}^{-2} \text{d}^{-1}$)	POC/PN
1	1 Dec 2017	1 Jan 2018	31	15.99	170.94	119.80	51.14	7.49
2	1 Jan 2018	1 Feb 2018	31	15.07	204.40	127.50	76.90	8.46
3	1 Feb 2018	8 Feb 2018	7	24.94	1213.58	314.95	898.63	12.63
4	8 Feb 2018	15 Feb 2018	7	37.39	330.00	250.04	79.95	6.69
5	15 Feb 2018	22 Feb 2018	7	20.71	270.10	174.29	95.81	8.41
6	22 Feb 2018	1 Mar 2018	7	40.28	387.68	214.59	173.08	5.33
7	1 Mar 2018	8 Mar 2018	7	12.29	193.80	77.39	116.42	6.30
8	8 Mar 2018	15 Mar 2018	7	23.32	211.04	155.25	55.79	6.66
9	15 Mar 2018	22 Mar 2018	7	21.47	247.39	134.37	113.02	6.26
10	22 Mar 2018	29 Mar 2018	7	110.38	898.30	709.40	188.90	6.43
11	29 Mar 2018	4 Apr 2018	7	76.27	863.06	585.00	278.06	7.67
12	4 Apr 2018	12 Apr 2018	7	85.25	834.83	625.45	209.38	7.34
13	12 Apr 2018	19 Apr 2018	7	148.40	1676.91	1238.63	438.28	8.35
14	19 Apr 2018	26 Apr 2018	7	88.63	720.50	570.07	150.43	6.43
15	26 Apr 2018	3 May 2018	7	68.44	687.71	587.03	100.67	8.58
16	3 May 2018	10 May 2018	7	61.29	832.17	498.94	333.23	8.14
17	10 May 2018	17 May 2018	7	186.82	2570.39	1601.51	968.89	8.57
18	17 May 2018	24 May 2018	7	83.26	749.61	572.77	176.85	6.88
19	24 May 2018	31 May 2018	7	42.84	424.12	326.40	97.71	7.62
20	31 May 2018	7 Jun 2018	8	27.41	221.31	198.58	22.73	7.24

Table S2. Characteristics of the theoretical footprint area integrated by the aquatic eddy covariance for each site based on the model parametrization by Berg et al. (2007). It shows the mean bottom roughness length scale (z_0), the footprint length (F_{length}) and width (F_{width}), region of maximum flux contribution (X_{max}) and overall footprint area (F_{area}) for each site. Note that the model was applied outside of the validated range ($z_0 \leq 1$ cm and measurement height ≤ 0.3 m). The resulting footprint estimates might therefore be subject to higher uncertainties.

Site	AEC Deployment	z_0 (cm)	F_{length} (m)	$F_{\text{width}}^{\text{a}}$ (m)	X_{max} (m)	$F_{\text{area}}^{\text{b}}$ (m ²)
Sand	AEC-1	0.8	56.9	2.3	2.4	102.2
Sand (off garden)	AEC-4	4.5	12.4	2.3	0.10	22.3
Coral garden	AEC-2	6.4	11.6	2.3	0.13	20.9
Coral garden	AEC-3	6.8	22.1	2.3	0.6	39.7
Coral garden	AEC-5	7.3	8.2	2.3	0.04	14.7

a: for a measurement height (h) of 0.35 m

b: approximated as an ellipsoid.

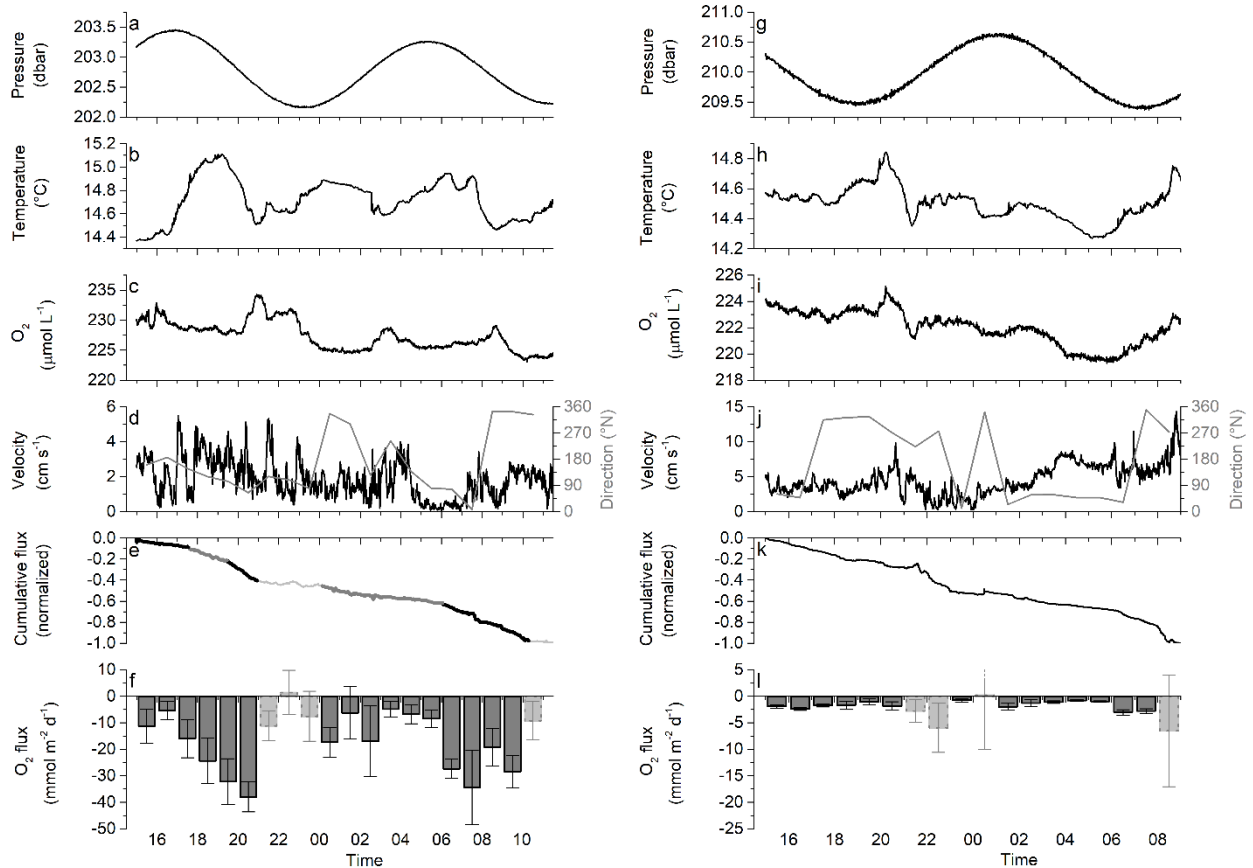


Figure S1. Example of aquatic eddy co-variance (AEC) dataset for the mixed coral garden (AEC-2; a – f) and sandy reference site (AEC-1; g – l). It shows time series of pressure (a, g), temperature (b, h), dissolved oxygen (O_2 ; c, i) from the SBE19 CTD probe, flow velocity and flow direction (gray line) from the acoustic Doppler velocimeter (d, j). Panels e, k, depict the normalized cumulative flux; periods with stable linear changes in the cumulative flux were used to characterize coral garden habitats, as exemplified by the grey and black lines in panel e (see Figure 3). Hourly O_2 flux averages with standard error are shown in panels f and l; averages from periods with unstable cumulative flux (light grey bars) were flagged and not included on the site's averages (see Table 2). Note that the observed correlation between temperature and O_2 during deployment AEC01 (panels h,j) and AEC03 (not shown) might have affected the obtained O_2 uptake. Given the reduced O_2 concentration changes over the deployment, however, the effect was deemed negligible.

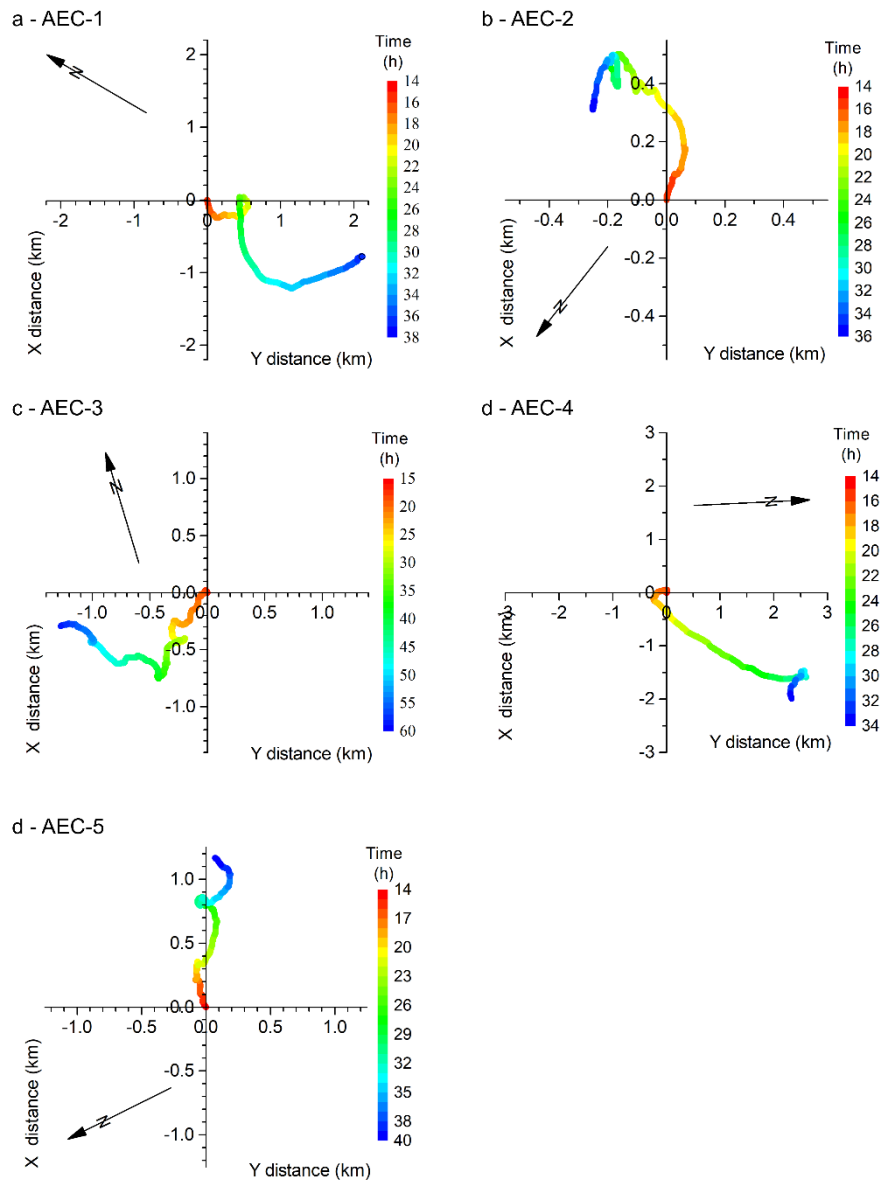


Figure S2. Theoretical two-dimensional particle track analysis for all AEC deployments. The travel distance along the ADV instrument coordinates X and Y are plotted at 1 min interval with the tracks color representing the deployment time in hours (starting at 00:00 of each deployment day). The arrows indicate the North direction in relation to the instrument coordinate system.

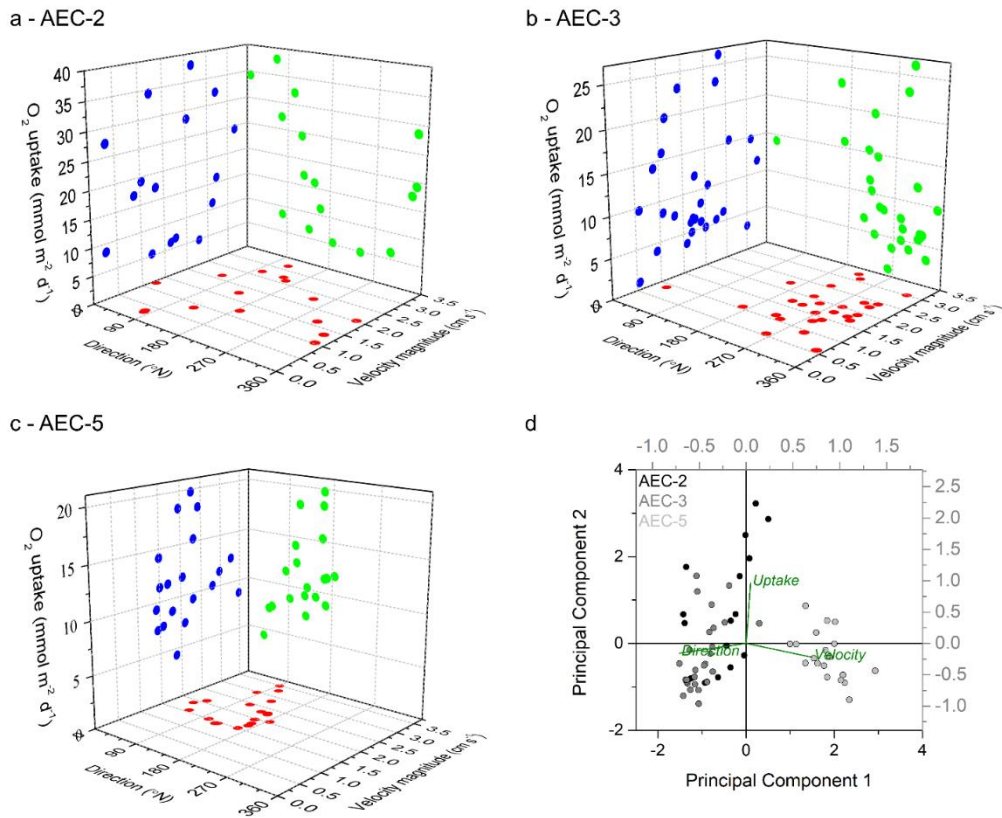


Figure S3. Correlation between O_2 uptake rates and flow velocity and direction. It shows three-dimensional correlation plots for AEC-2 (a), AEC-3 (b), and AEC-5 (c) based on hourly O_2 uptake averages and associated flow characteristics. (d) Correlation-based principal components analysis of the data shown on panels a-c. Note that the principal component 1 (PC1) is mostly driven by hydrodynamics, with principal component 2 (PC2) being mostly driven by changes in O_2 uptake. PC1 and PC2 explained 58.3% and 35.3% of the data variance, respectively.

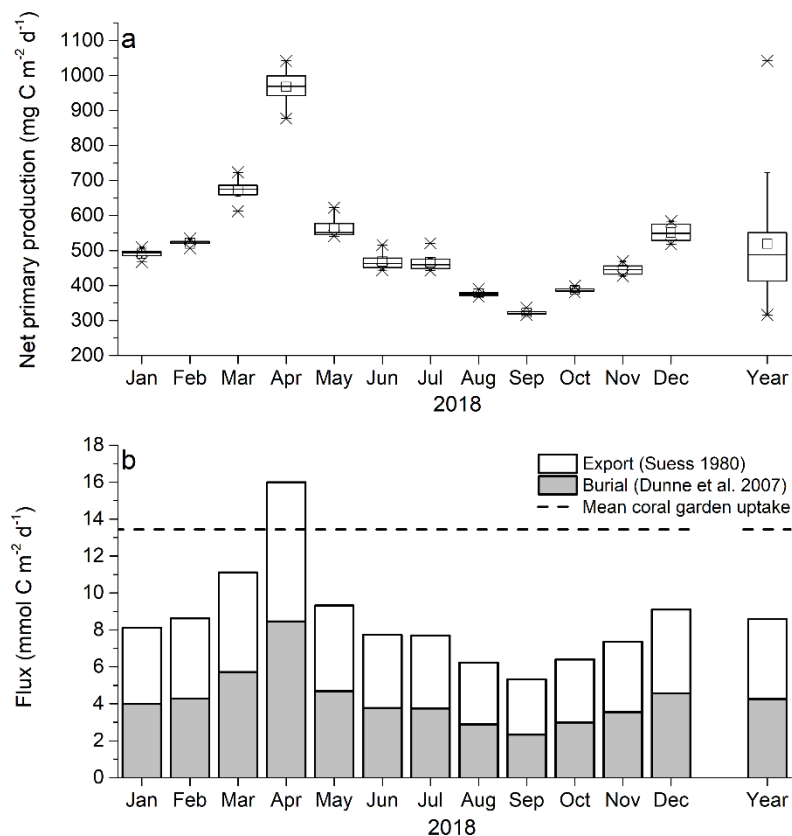


Figure S4. (a) Mean monthly estimates of net primary production (NPP) within the Condor seamount region (latitude $38^{\circ} 27'$ to $38^{\circ} 36'$ N and longitude $28^{\circ} 51'$ to $29^{\circ} 9'$ W) for 2018 obtained from the Ocean Productivity repository (Oregon State University; <http://sites.science.oregonstate.edu/ocean.productivity>), quantified from MODIS-based remote sensing estimates of ocean surface chlorophyll a concentrations using the Vertically Generalized Production Model (VGPM; Behrenfeld & Falkowski 1997). Note that the obtained NPP values were averaged per month and for the whole 2018 to better highlight seasonal variabilities. (b) Flux of particulate organic carbon (POC) reaching the summit of the seamount from export of NPP estimated after Suess (1980) together with the proportion of POC burial (after Dunne et al. (2007)). The mean uptake rate for the coral garden in this study is expressed in $\text{mmol C m}^{-2} \text{d}^{-1}$ assuming a 1:1 carbon to O_2 ratio (see Glud 2008).

References

- Behrenfeld MJ, Falkowski PG (1997) Photosynthetic rates derived from satellite-based chlorophyll concentration. *Limnol Oceanogr* 42:1–20.
- Berg P, Roy H, Wiberg PL (2007) Eddy correlation flux measurements: The sediment surface area that contributes to the flux. *Limnol Oceanogr* 52:1672–1684.
- Dunne JP, Sarmiento JL, Gnanadesikan A (2007) A synthesis of global particle export from the surface ocean and cycling through the ocean interior and on the seafloor. *Global Biogeochem Cycles* 21:Gb4006.
- Glud RN (2008) Oxygen dynamics of marine sediments. *Mar Biol Res* 4:243–289.
- Suess E (1980) Particulate Organic-Carbon Flux in the Oceans - Surface Productivity and Oxygen Utilization. *Nature* 288:260–263.